[UCI]I804:24011-200000234255

2007. 02

Master's Thesis

A Study on Thermal Behavior and Mechanical characteristics in Hybrid welding (Nd:YAG Laser+MIG) of Al-Mg-Si alloys

Graduate School of Chosun University

Department of Naval Architecture and Ocean Engineering

Jeong Eun-Young

A Study on Thermal Behavior and Mechanical characteristics in Hybrid welding (Nd:YAG Laser+MIG) of Al-Mg-Si alloys

하이브리드(Nd:YAG+MIG) 용접을 이용한
알루미늄(Al-Mg-Si)합금의 열적 거동 및 역학적 특성에
관한 연구

February 2007

Graduate School of Chosun University

Department of Naval Architecture and
Ocean Engineering

Jeong Eun-Young

A Study on Thermal Behavior and Mechanical characteristics in Hybrid welding (Nd:YAG Laser+MIG) of Al-Mg-Si alloys

Advisor : Professor Han-Sur Bang

A Thesis submitted for the degree of

Master of Engineering

October 2006

Graduate School of Chosun University

Department of Naval Architecture and

Ocean Engineering

Jeong Eun-Young

鄭垠永의 碩士學位 論文을 認准함

委員長 朝鮮大學校 敎授 房 熙 善

委 員 朝鮮大學校 敎授 房 漢 瑞

委 員 朝鮮大學校 敎授 尹 德 榮

2006 年 11 月 30日

朝鮮大學校大學院

CONTENTS

ABSTRACT

A Study on Thermal Behavior and Mechanical characteristics in Hybrid welding (Nd:YAG Laser+MIG) of Al-Mg-Si alloys

Jeong Eun-Young
Advisor : Prof. Bang Han-Sur Ph.D.
Department of Naval Architecture & Ocean Engineering,
Graduate School of Chosun University

Presently the consumption and application of aluminum alloys has been increased in many industrial fields, aerospace, automobiles, shipbuilding, electronics, building constructions etc. for light in weight and high strength. Therefore welding technology of aluminum alloys has already become a most important problem in industrial settings.

Aluminum alloys are light in weight materials suitable for high-speed and durability because it has a high ratio of strength to density, corrosion resistance, good toughness and metallurgical characteristics at low temperature. For example 5xxx and 6xxx series of aluminum alloys has been raised in shipbuilding due to distinguished corrosion resistance, and they are not affected by big difference of salinity or temperature.

However aluminum alloys are very active materials and has high thermal conductivity and thermal expansion coefficient. So welding defects and deformation can be generated by the high hydrogen solubility between liquid-state and solid-state. Thus when welding of aluminum alloys, high heat input and current are required in a short time.

According to increase in use of aluminum alloys, new welding technology has been required for improvement of productivity and quality, while making up the weak points of conventional welding method and process.

In this study new joining technology, laser+arc hybrid welding, was introduced and observed the weldability and feasibility in aluminum alloys for complementing the disadvantages of conventional arc welding. The 6xxx series of aluminum alloys were butt jointed by CW 3kW Nd:YAG laser+MIG hybrid welding.

Firstly characteristics of thermal distribution and residual stress distribution in weldment by hybrid welding were surveyed using numerical analysis. Secondly the optimum parameters of hybrid welding were determined based on experiments. And mechanical testing and residual stress measurement were carried out and compared with the numerical analysis.

In conclusion, application possibility of laser+arc hybrid welding to aluminum alloys are confirmed.

List of Figure

List of Table

CHAPTER 1. Introduction

1.1 Backgrounds & Purposes

Aluminum alloys are light in weight and high strength, and have the ratio of density to strength, corrosion resistance, toughness, good formability and weldability. Therefore it has been used in many fields of structural, architectural, automotive, railway, and marine applications.[1]

Aluminum alloys are joined with most of the known joining process. In many instances, aluminum alloys are joined by conventional equipment and techniques used with other metals, usually MIG welding. Occasionally, specialized equipment or techniques, or both, are required.

The reason that specialized equipment or techniques are necessary is physical and metallurgical characteristics of aluminum alloys. Especially important characters of aluminum alloys are high thermal and electrical conductivity, and thermal expansion coefficient. These characteristics make aluminum alloys deformed while welding.

High thermal conductivity (as compare to steel) necessitates a high rate of heat input for fusion welding of aluminum alloys. Thick sections may even require preheating. Aluminum's high thermal and electrical conductivities require high current, shorter weld time, and more precise control of the welding variables than steel.[2]

Also welding construction, deformation controlling technology, technical experts and information of aluminum welding, aluminum material property details, equipments and components related to aluminum welding are insufficient.

Laser-MIG hybrid welding is a completely innovative technology that offers synergies for wide fields of application in automotive, shipbuilding, aerospace etc. compared to single process. This technology specializes in that advantages of each welding process can be maximized in concurrence with complementing the disadvantages.

Due to these merits, many industrial companies in developed countries has been investigating and applying the hybrid welding process.

MIG welding can weld large joints gaps comparatively, and control the chemical composition of weldment using filler wire. Welding deformation, however, can be occurred by slow welding speed and high heat input producing a wide and shallow weld.

Laser welding focuses the beam in high density and joins the materials. Very deep penetration and narrow heat affected zone (HAZ) can be obtained. Welding deformation can be also minimized due to concentrated high heat input density. But the critical problem of laser welding is that gap bridging capability is much less than MIG welding. Because diameter of laser beam is too small, an exact joint preparation and clamping are needed. Also metal composition cannot be controlled by filler wire.

Along with conquest of faults in two welding process, laser-MIG hybrid welding can be realized by good points of laser and MIG welding process in one welding zone, like a good bridging ability, high travel speed, deep penetration and improved process stability etc.

Finally laser+MIG hybrid welding can improve the aluminum welding and reduce the welding deformation.

Many welding process phenomena and mechanical experiments of hybrid welding have been studied for a long time. On the other hands, researches on characteristics of hybrid welding heat source have been investigated but it leaves much to be desired. So in this study, characteristics of heat source in laser+MIG hybrid welding were inquired by numerical analysis and compared to experimental results.

Arc welding process

1. **Good gap tolerance**
2. **Inexpensive**
3. **Metallurgical control**
4. **High energy efficiency (~80%)**
5. Small energy density
6. Limited penetration

+

Laser welding process

1. **Deep & narrow weld**
2. **Great beam penetration**
3. **Fast welding speed**
4. **High energy density**
5. Low energy efficiency (~10%)
6. Bad gap tolerance
7. Expensive (high power)

⇩

Hybrid welding process

1. **Higher process stability**
2. **Higher welding speed**
3. **Great welding depth**
4. **Good bridge ability**
5. **Good metallurgical properties**

Fig. 1.1 Synergy effects of Laser+Arc hybrid welding process

1.2 Materials Used

Aluminum alloys have low density, non-magnetic and electricity is four times, coefficient of linear expansion is twice higher than steel. Due to these characteristics, high heat input required by fast heating and cooling in non-equilibrium state of aluminum results in welding deformations. Hence these characteristics are the most important factors when deciding weldability in fusion welding of aluminum alloys.

Aluminum alloys are classified according to a kind of elements. Generally various kinds of elements have been inserted with aluminum for promoting strength by precipitation hardening, because strength of pure aluminum is low. Besides, aluminum alloys are divided into two classes by the method of heat treatment, heat-treatable alloys and non-heat-treatable alloys. Among heat-treatable alloys, it is divided into O, T6, T4 etc. and non-heat-treatable alloys are also divided into H11, H12 according to the heat treatment way.
As it mentioned purposes of this study, 6xxx series, exactly A6061-T6, were used in experiments.

Although not as strong as most 2xxx and 7xxx alloys, 6xxx series alloys have good formability, weldability, machinability, and corrosion resistance, with medium strength. Mechanical properties of A6061 are shown in Table1.1 .[3]

Table 1.1 Mechanical Properties of A6061[4]

Al Alloy	Ultimate Tensile Strength		Yield Strength	
	Mpa	ksi	Mpa	ksi
6061-T6	310	45	276	40

Alloys in the 6xxx series contain silicon and magnesium approximately in the proportions required for formation of magnesium silicide (Mg_2Si), thus making them heat treatable. Table1.2 shows chemical compositions of A6061.

Table 1.2 Chemical compositions of A6061(%)[5]

Al Alloy	Si	Fe	Cu	Mn	Mg	Cr	Zn	others	Al
A6061	0.40~ 0.8	0.7	0.15 ~0.40	0.15	0.8 ~1.2	0.04 ~0.35	0.25	0.15	Rem

Generally filler wire should be similar with base metal. Joint strength, corrosion resistance, ductility and toughness are determined by base metal and filler wire. In case of heat-treatable aluminum alloys, filler wire which has alloying elements more than base metal is used for decreasing hot cracking susceptibility occurred easily in aluminum welding. Therefore A4043 or A5356 which have Si or Mg more than A6061 are good for filler wires in A6061 welding.[6] In this study, A4043 was used for filler wire. Table 1.3 shows chemical compositions of A4043.

Table 1.3 Chemical compositions of A4043(%)

Al Alloy	Si	Fe	Cu	Mn	Mg	Zn	Ti	others	Al
Al 4043	4.5 ~6.0	0.8	0.30	0.05	0.05	0.10	0.20	0.15	Rem

1.3 Organizations & Scope of Study

As increasing the use of aluminum alloys, it is obviously certain that an improvement of aluminum welding is needed. And for meeting this demand, it has come out that hybrid welding could be applied in the manufacturing fields of aluminum alloys and many researches in this field has been carried out. But a study in regard to heat sources of hybrid welding has not yet been investigated.

Therefore, in this study, fundamental information about heat source of hybrid welding used for its numerical simulation and various experiments on hybrid welding have been performed.

For analyzing the heat source of laser+MIG hybrid welding, basic theory of heat transfer was formulated using finite element method(FEM). A previously developed heat source model of laser+MIG hybrid welding has been used to carry out the heat transfer analysis and determine the thermal history. Also residual stress distribution was analyzed and compared with measured residual stress values.

Aluminum alloys were jointed by laser+MIG hybrid welding and the weldments were observed. Finally experimental results of laser+MIG hybrid welding were compared with results of numerical simulation.

CHAPTER 2. Numerical Simulation of Hybrid welding

2.1 Theoretical Basis for Analysis

2.1.1 Heat Transfer Analysis

Fourier's law is an empirical law based on observation. It states that the rate of heat flow, dQ/dt, through a homogeneous solid is directly proportional to the area, A, of the section at right angles to the direction of heat flow, and to the temperature difference along the path of heat flow, dT/dx i.e.

$$q = -\lambda_x \frac{dT}{dx} \tag{2.1}$$

So for 3D-case the rate of heat transfer is

$$\frac{\partial}{\partial x}\left(\lambda_x \frac{\partial T}{\partial x}\right) + \frac{\partial}{\partial y}\left(\lambda_y \frac{\partial T}{\partial y}\right) + \frac{\partial}{\partial z}\left(\lambda_z \frac{\partial T}{\partial z}\right) \tag{2.2}$$

The thermal analysis was conducted using temperature dependent thermal material properties. From conservation of energy the governing equation of heat conduction in weldment is obtained as (considering the medium to be isotropic)

$$\rho c \frac{\partial T}{\partial t} = \lambda\left(\frac{\partial^2 T}{\partial x^2} + \frac{\partial^2 T}{\partial y^2} + \frac{\partial^2 T}{\partial z^2}\right) + \dot{Q} \tag{2.3}$$

where

T : Temperature (℃)

ρ : Density (g/cm^3)

$\dot{Q}$: Rate of temperature change due to heat generation per volume (cal/cm^3· sec)

t : Time (sec)

λ : Thermal conductivity of isotropic material (cal/cm^3· sec· ℃)

c : Specific heat (cal/g· ℃).

Boundary condition to solve the equation (2.3) is given in the following form using the heat flux q (cal/cm^3· sec· ℃) in normal direction on the boundary of the object.

$$q = -\lambda \frac{\partial T}{\partial n} \tag{2.4}$$

Heat conduction problem for the object of analysis is formulated as the finite element method using Galerkin method. Internal temperature of the element, T, is given by

$$T(x, y, z, t) = [N(x, y, z)]\{\phi(t)\} \tag{2.5}$$

where $[N]$ is a shape function matrix shown the relation between nodal temperature and internal temperature of the element. $\{\phi\}$ is the vector of the nodal temperature of the element at time t.

If Galerkin method is applied in equation (2.3) using $[N]$ as a weighting function at this time, following equation is obtained.

$$\int_{V^e} [N]^T \left\{ \lambda \left(\frac{\partial^2 T}{\partial x^2} + \frac{\partial^2 T}{\partial y^2} + \frac{\partial^2 T}{\partial z^2} \right) + \dot{Q} - \rho c \frac{\partial T}{\partial t} \right\} dV = 0 \tag{2.4}$$

where superscript, T, shows transformation of matrix and subscript, V^e, shows the domain of element. The term of second order in partial differential equation (2.6) is changed using Green-Gauss theorem, a formula of partial integration, to the following equation.

$$\int_{V^e} \lambda \left(\frac{\partial [N]^T}{\partial x} \frac{\partial [N]}{\partial x} + \frac{\partial [N]^T}{\partial y} \frac{\partial [N]}{\partial y} + \frac{\partial [N]^T}{\partial z} \frac{\partial [N]}{\partial z} \right) dV \bullet \{\phi(t)\} \tag{2.7}$$
$$+ \int_{V^e} \rho c [N]^T [N] dV \bullet \frac{\partial \{\phi(t)\}}{\partial t} = \int_{V^e} \dot{Q} [N]^T dV - \int_{S^e} q [N]^T dS$$

Simplifying above equation (2.7), un-stationary heat conduction problem can be expressed as following finite element expression for an element.

$$[k]\{\phi\} + [c]\left\{ \frac{\partial \phi}{\partial t} \right\} = \{f\} \tag{2.8}$$

where $[k]$, $[c]$ and $\{f\}$ show the heat conductivity matrix of an element, the heat capacity matrix of an element and the heat flow vector of an element, respectively. They are expressed as follows:

$$[k] = \int_{V^e} \lambda \left(\frac{\partial [N]^T}{\partial x} \frac{\partial [N]}{\partial x} + \frac{\partial [N]^T}{\partial y} \frac{\partial [N]}{\partial y} + \frac{\partial [N]^T}{\partial z} \frac{\partial [N]}{\partial z} \right) dV \tag{2.9}$$

$$[c] = \int_{V^e} \rho c [N]^T [N] dV \tag{2.10}$$

$$\{f\} = \int_{V^e} \dot{Q} [N]^T dV - \int_{S^e} q [N]^T dS \tag{2.11}$$

Finite element formula for the whole object analysed is constructed with assembled each matrix of elements and it can be expressed as follows:

$$[K]\{\Phi\}+[C]\left\{\frac{\partial \Phi}{\partial t}\right\}=\{F\} \tag{2.12}$$

where $[\Phi]$, $[K]$, $[C]$ and $\{F\}$ show the vector of the nodal temperature in the whole object, the heat conductivity matrix in the whole object, the heat capacity matrix in the whole object and the heat flow vector in the whole object, respectively.

2.1.2 Thermal elasto-plastic analysis

A. Basic theory for thermal stress analysis by finite element method

The increment of strain in the element is given by appropriate differentiation of the internal displacements as shown in bellows.

$$\{d\varepsilon\} = [B]\{dw\} \tag{2.13}$$

The increment of stress in element is obtained by using an appropriate matrix $[D]$, the elasticity matrix $[D^e]$ or the plasticity matrix $[D^p]$, and the increment of strain.

$$\{d\sigma\} = [D]\{d\varepsilon\} \tag{2.14}$$

If the increment of initial strain $\{d\varepsilon_0\}$ exists, increment of stress is expressed as follows.

$$\{d\sigma\} = [D]\{d\varepsilon - d\varepsilon_0\} \tag{2.15}$$

where the initial strains are function of temperature such as thermal strains and has the following relation.

$$\{d\varepsilon_0\} = \{d\varepsilon^T\} = \{\alpha\}dT \tag{2.16}$$

Using this relation, the increment of stress, equation (2.15), can be rewritten in the following form.

$$\{d\sigma\}=[D]\{d\varepsilon\}-[C]dT \tag{2.17}$$

The relationship between the increment of the nodal force, $\{dF\}$, and the nodal displacement, $\{dw\}$, is obtained by applying the principle of virtual work as bellows.

$$\begin{aligned}\{dF\}&=\int[B]^T[D]\{d\varepsilon\}dV-\int[B]^T[C]dTdV \\ &\equiv[K]\{dw\}-\{dL\}\end{aligned} \tag{2.18}$$

where

$$[K]=\int[B]^T[D]\{d\varepsilon\}dV \text{ - The stiffness matrix} \tag{2.19}$$

$$\{dL\}=\int[B]^T[C]dTdV \text{ - The nodal force due to initial strain} \tag{2.20}$$

The equilibrium state of the whole object will be kept in satisfying the additional equilibrium condition at each step of temperature increments which are constituted with individual equilibrium equation at each node as follows.

$$\sum\{dF\}=\sum[K]\{dw\}-\sum\{dL\} \tag{2.21}$$

If there is no external force acting at the nodes, the above equation is expressed in the simple form as bellows.

$$\sum\{dL\}=\sum[K]\{dw\} \tag{2.22}$$

For the $[D]$ and $[C]$, it will be obtained from stress-strain relation in elastic and plastic range as shown in next.

B. Stress and strain relation dependent upon temperature

1) Stress-strain relation in elastic range

In the elastic range, the increment of total strain consists of increment of elastic strain $\{d\varepsilon^e\}$ and the increment of thermal expansion strain $\{d\varepsilon^T\}$ as bellows.

$$\{d\varepsilon\} = \{d\varepsilon^e\} + \{d\varepsilon^p\} \tag{2.23}$$

The increment of thermal expansion strain is expressed using the coefficient of linear expansion.

$$\{d\varepsilon^T\} = \{\alpha\} dT \tag{2.24}$$

When the elasticity matrix, $[D^e]$, changes as temperature increase, the increment of elastic strain is given in the following form.

$$\begin{aligned} \{d\varepsilon^e\} &= [D^e]^{-1}\{d\sigma\} + \frac{\partial [D^e]^{-1}}{\partial T}\{\sigma\} dT \\ &\equiv \{d\varepsilon^{e'}\} + \{d\varepsilon^{T'}\} \end{aligned} \tag{2.25}$$

Transposing $\{d\sigma\}$ in above equation, the increment of stress is given by

$$\{d\sigma\} = [D^e]\{d\varepsilon^e\} - [D^e]\frac{\partial [D^e]^{-1}}{\partial T}\{\sigma\} dT \tag{2.26}$$

Substituting equation (2.25) into equation (2.23), the increment of strain is given by

$$\{d\varepsilon\}=[D^e]^{-1}\{d\sigma\}+\frac{\partial[D^e]^{-1}}{\partial T}\{\sigma\}dT+\{\alpha\}dT \tag{2.27}$$

Substituting of equation (2.24) and (2.27) into equation (2.26) becomes

$$\{d\sigma\}=\underbrace{[D^e]}_{[D]}\{d\varepsilon\}-\underbrace{[D^e]\left(\{\alpha\}+\frac{\partial[D^e]^{-1}}{\partial T}\{\sigma\}\right)}_{[C]}dT=[D^e]\{d\varepsilon^{e'}\} \tag{2.28}$$

From this equation, the required matrix $[D]$ and $[C]$ in equation (2.17) are obtained.

2) Stress-strain relation in plastic range

Yield of materials is occurred when its yield function, f, satisfy the following equation.

$$f=0 \tag{2.29}$$

According to the associated flow rule (increment theory of plasticity), the increment of plastic strain, $\{d\varepsilon^p\}$, is given in following form.

$$\{d\varepsilon^p\}=\lambda\left\{\frac{\partial f}{\partial\sigma}\right\} \tag{2.30}$$

where f is plastic potential and λ is a positive scalar.

In the elasto-plastic problem, the total increment of strain is consisted of the summation of increment in elastic strain, plastic strains and thermal strains as follows.

$$\{d\varepsilon\} = \{d\varepsilon^e\} + \{d\varepsilon^p\} + \{d\varepsilon^T\} \tag{2.31}$$

Above equation is changed using the equation (2.25) as bellows.

$$\{d\varepsilon\} = \{d\varepsilon^{e'}\} + \{d\varepsilon^p\} + \{d\varepsilon^T\} + \{d\varepsilon^{T'}\} \tag{2.32}$$

Form the equation (2.26), following equation is obtained using

$$\begin{aligned}\{d\sigma\} &= [D^e](\{d\varepsilon\} - \{d\varepsilon^p\} - \{d\varepsilon^T\}) - [D^e]\frac{\partial [D^e]^{-1}}{\partial T}\{\sigma\}dT \\ &= [D^e]\{d\varepsilon\} - [D^e]\lambda\left\{\frac{\partial f}{\partial \sigma}\right\} - [D^e]\left(\{\alpha\} + \frac{\partial [D^e]^{-1}}{\partial T}\{\sigma\}\right)dT\end{aligned} \tag{2.33}$$

If the material is under loading in the plastic range, the following condition should be satisfied.

$$0 = df = \left\{\frac{\partial f}{\partial \sigma}\right\}^T \{d\sigma\} + \left\{\frac{\partial f}{\partial \varepsilon^p}\right\}^T \{d\varepsilon^p\} + \frac{\partial f}{\partial T}dT \tag{2.34}$$

Substitution of equation (2.33) into equation (2.34) gives

$$\begin{aligned}0 = &\left\{\frac{\partial f}{\partial \sigma}\right\}^T \left([D^e]\{d\varepsilon\} - [D^e]\lambda\left\{\frac{\partial f}{\partial \sigma}\right\} - [D^e]\left(\{\alpha\} + \frac{\partial [D^e]^{-1}}{\partial T}\{\sigma\}\right)dT\right) \\ &+ \left\{\frac{\partial f}{\partial \varepsilon^p}\right\}^T \lambda\left\{\frac{\partial f}{\partial \sigma}\right\} + \frac{\partial f}{\partial T}dT\end{aligned} \tag{2.35}$$

Above equation can be rearranged in the following form.

$$\lambda=\frac{\left\{\frac{\partial f}{\partial\sigma}\right\}^T[D^e]\{d\varepsilon\}-\left\{\frac{\partial f}{\partial\sigma}\right\}^T[D^e]\left(\{\alpha\}+\frac{\partial[D^e]^{-1}}{\partial T}\{\sigma\}\right)dT+\frac{\partial f}{\partial T}dT}{\left\{\frac{\partial f}{\partial\sigma}\right\}^T[D^e]\left\{\frac{\partial f}{\partial\sigma}\right\}-\left\{\frac{\partial f}{\partial\varepsilon^p}\right\}^T\left\{\frac{\partial f}{\partial\sigma}\right\}} \quad (2.36)$$

Form the substitution of above equation into equation (2.33), equation (2.33) rearranged as follows and it shows the relation between the increments of stress and total strain in the plastic range.

$$\{d\sigma\}=[D^e]\{d\varepsilon\}-\left([D^e]\{\alpha\}+[D^p]\frac{\partial[D^e]^{-1}}{\partial T}\{\sigma\}+[D^e]\left\{\frac{\partial f}{\partial\sigma}\right\}\frac{\partial f}{\partial T}/S\right)dT$$

(2.37)

where $[D^p]$ is the plasticity matrix and is expressed as bellows.

$$[D^p]=[D^e]-[D^e]\left\{\frac{\partial f}{\partial\sigma}\right\}\left\{\frac{\partial f}{\partial\sigma}\right\}^T[D^e]/S \quad (2.38)$$

$$S=\left\{\frac{\partial f}{\partial\sigma}\right\}^T[D^e]\left\{\frac{\partial f}{\partial\sigma}\right\}-\left\{\frac{\partial f}{\partial\sigma}\right\}^T\left\{\frac{\partial f}{\partial\sigma}\right\} \quad (2.39)$$

Then, the required matrix $[D]$ and $[C]$ to solve the equation (2.29) are shown to be

$$[D]=[D^p] \quad (2.40)$$

$$[C]=[D^e]\{\alpha\}+[D^p]\frac{\partial[D^e]^{-1}}{\partial T}\{\sigma\}+[D^e]\left\{\frac{\partial f}{\partial\sigma}\right\}\frac{\partial f}{\partial T}/S \quad (2.41)$$

When λ is found to be negative ($\lambda<0$) during the computation, the material is subjected to unloading.

At this condition, the increment relation of stress and strain should be replaced by equation (2.28) instead of equation (2.37).[7]

C. Temperature dependency of material properties

In this study, temperature dependency of material properties has been considered all over the elastic and plastic fields. Fig. 2.1 and Fig. 2.2 shows the temperature dependent mechanical and physical properties of A6061-T6.

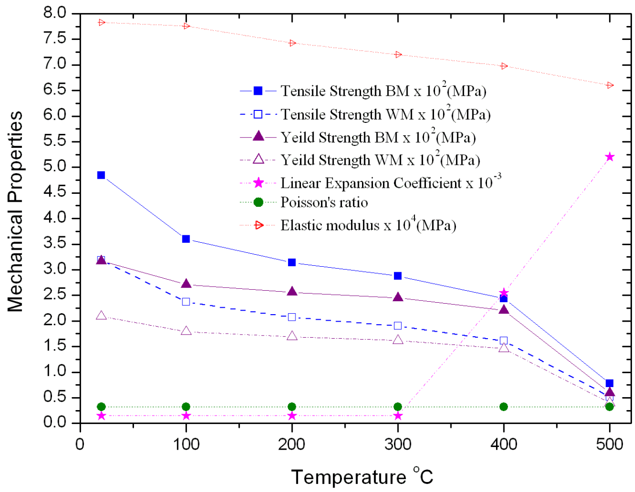

Fig. 2.1 Mechanical properties of A6061-T6

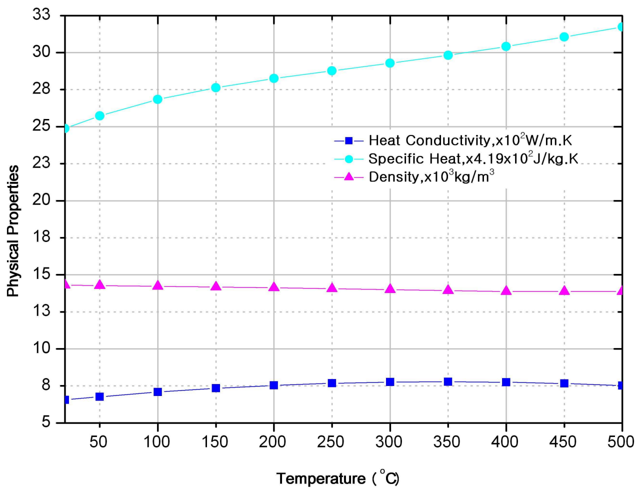

Fig. 2.2 Physical Properties of A6061-T6

2.2 Analysis Conditions and FE Model of Hybrid welding

2.2.1 Analysis Conditions

Based on basic theory of heat transfer has been discussed in this chapter. The spatial and temporal temperature distribution satisfies the governing equation of unstationary heat conduction. Welding heat source is assumed as an instantaneous heat source and two dimensional four-noded isoparametric element is used.

Boundary conditions are such that heat transfer exists inside the heat source model and atmosphere. The material is assumed as an isotropic material. The workpiece is initially at 20℃. Convective flow in the weld pool, vaporization in the keyhole and radiation heat transfer was not considered. Fig. 2.3 shows the boundary condition for heat conduction and thermal elasto-plastic analysis.

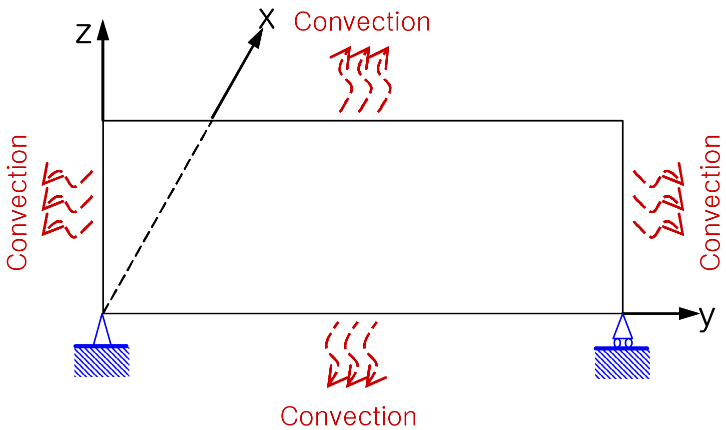

Fig. 2.3 Boundary conditions for **Heat conduction** and **Thermal elasto-plastic** analysis

Nominal dimension of specimen used was taken as 200×250×5mm

($W \times L \times T$) considering the effect of thermal shrinkage and expansion.

The schematic of the workpiece is shown in Fig. 2.4. A graded meshing is provided so that weld zone mesh size was 0.5mm×0.5mm and mesh size gradually increase toward transverse direction.

The total number of element were 1140, and 1265 nodes. Fig. 2.5 shows the mesh division used for the heat transfer and residual stress analysis of hybrid welding.

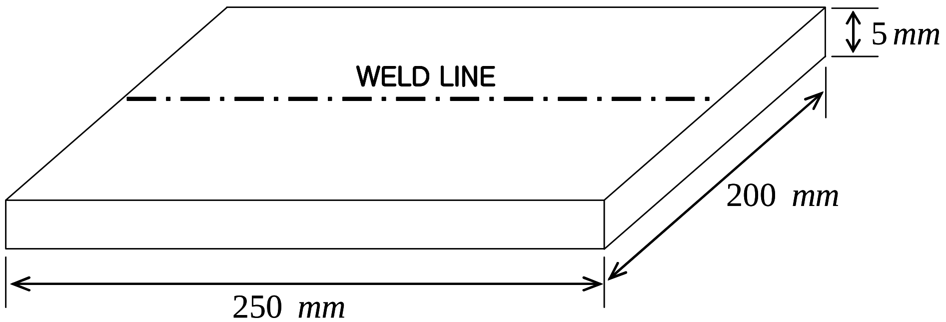

Fig. 2.4 Dimension of specimen for analysis (A6061-T6)

Fig. 2.5 2-D Mesh division of butt welded specimen by hybrid welding

Also temperature dependent material properties like thermal conductivity, specific heat, heat transfer coefficient, density, elastic modulus, yield strength, etc. are considered as described previously.

2.2.2 FE model for Hybrid welding

The welding heat source for analysis can be sorted out non-split type and split type as shown in Fig. 2.6. Non-split type has uniform flux (CASE.1) and split type is divided into volume-volume heat source (CASE.2) and volume-surface heat source (CASE.3). In this study CASE.2 was selected for analysis because it was proved that CASE.2 is proper method for heat source analysis of hybrid welding. Fig. 2.7 is schematic diagram of heat source.[8]

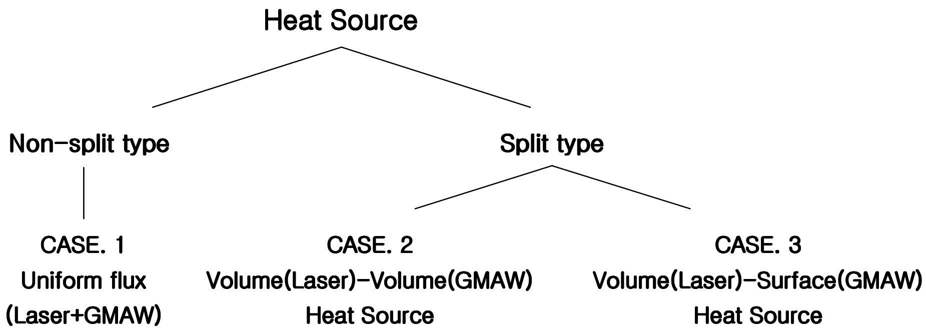

Fig. 2.6 Heat sources for analysis

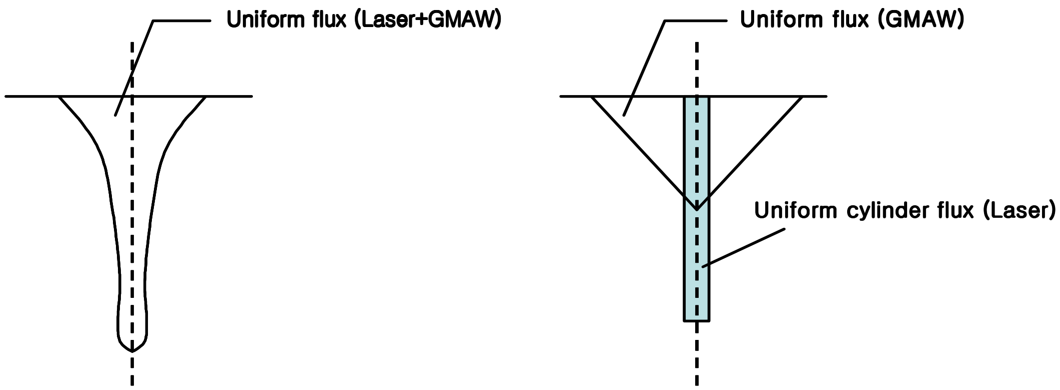

(1) Volume heat source (2) Volume-Volume heat source

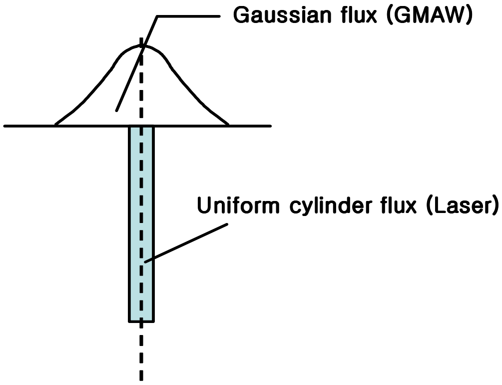

(3) Volume-Surface heat source

Fig. 2.7 Schematic diagram of heat source

Fig. 2.8 is the 2-D model for heat source analysis of hybrid welding. It shows a coupled model of laser and arc.

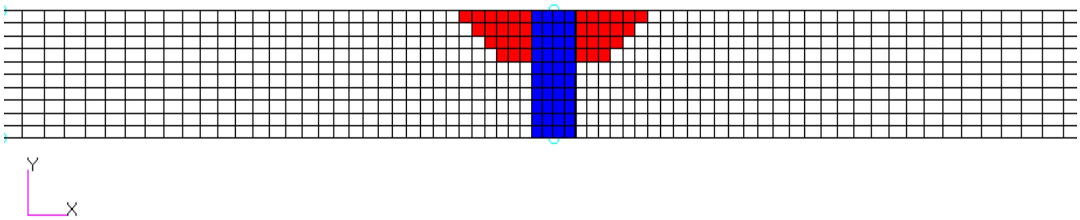

Fig. 2.8 Finite element model of heat source in laser+MIG hybrid welding

2.2.3 Calculation of Heat Input for Analysis of Hybrid welding

A. Gas Metal Arc welding

Heat input equation used in numerical simulation of GMAW is,

$$Q = \eta_A \frac{VI}{W_S} \tag{2.42}$$

where

Q : Heat input
η_A : Efficiency of arc welding
V : Arc Voltage (V)
I : Arc Current (A)
W_S : Welding speed (cm/sec)

Simulation conditions for GMAW are shown in Table 2.1. Efficiency of arc welding was 85%.[7]

Table 2.1 Welding conditions for simulation in GMAW

Welding Conditions	Current(A)	Arc voltage(V)	Welding speed (m/min)	Efficiency of arc welding (η_A)
	195 A	26V	0.85m/min	85%

B. Laser welding

Heat input equation used in numerical simulation of laser welding is,

$$Q = \eta_L \frac{P}{W_S} \tag{2.43}$$

where

η_L : Efficiency of laser welding

P : Laser power (kW)

W_S : Welding speed (cm/sec)

Simulation conditions for CW Nd:YAG laser are shown in Table 2.2. Efficiency of Nd:YAG laser welding fixed 35% which was calculated considering total absorption and losses of Nd:YAG laser beam.[7]

Table 2.2 Welding conditions for simulation in CW Nd:YAG laser

Welding Conditions	Laser power (kW)	Welding speed (m/min)	Efficiency of Nd:YAG laser welding (η_L)
	3kW	0.85m/min	35%

2.3 Results of Numerical Simulation in Hybrid welding

2.3.1 Heat Distribution characteristics of Hybrid welding

A phenomenon of heat transfer in laser+MIG hybrid welding is shown in Fig. 2.9. Centering around the welding heat source, welding heat is transferred from fusion zone to base metal. This temperature contour is also compared with the experimental results in Chapter 4.

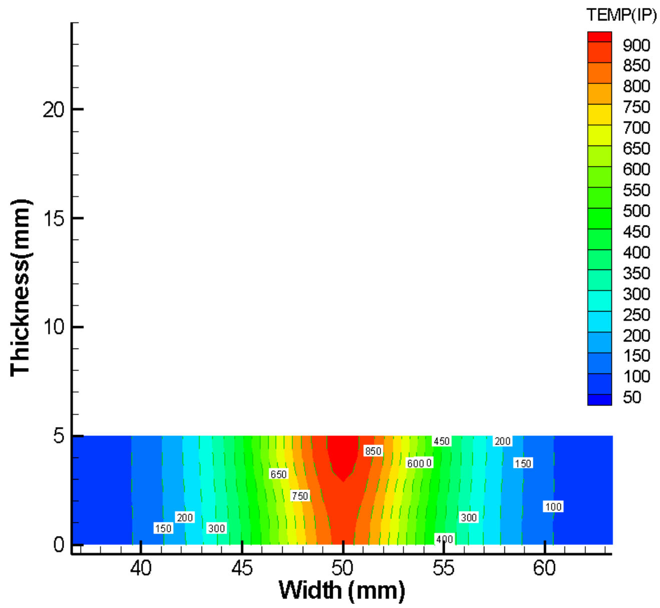

Fig. 2.9 Temperature contour of 0.5mm gap in hybrid welding

Fig. 2.10 shows the thermal history curve of fusion zone and HAZ. Maximum temperature was discovered after t=1.8sec. Maximum temperature was approximately 850℃ in fusion zone, 550℃ in HAZ from the thermal history curve, high temperature gradient was observed near the HAZ, which has relations to the rapid cooling rate in the case of laser welding.

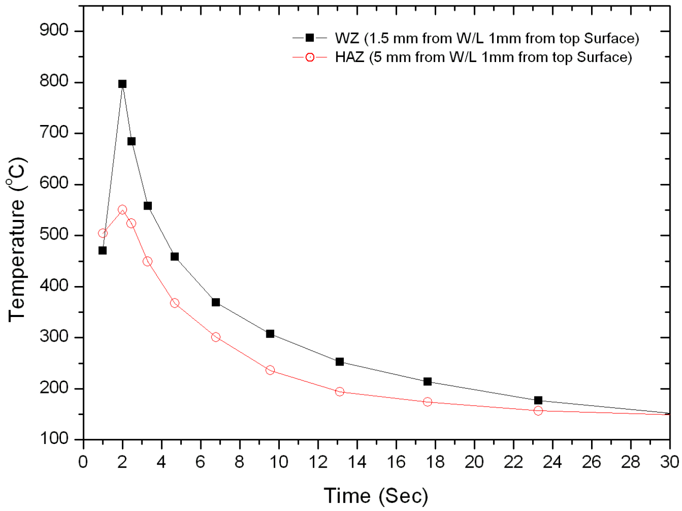

Fig. 2.10 Thermal history of 0.5mm gap in hybrid welding

2.3.2 Residual Stress characteristics of Hybrid welds

Residual stress was measured in longitudinal direction of hybrid welds. It has been confirmed that results of numerical simulation was almost accord with experimental results. Compressive residual stress occurred near HAZ and tensile residual stress was in fusion zone. Maximum residual stress value was 68Mpa that is about 25% of yield strength of A6061-T6.

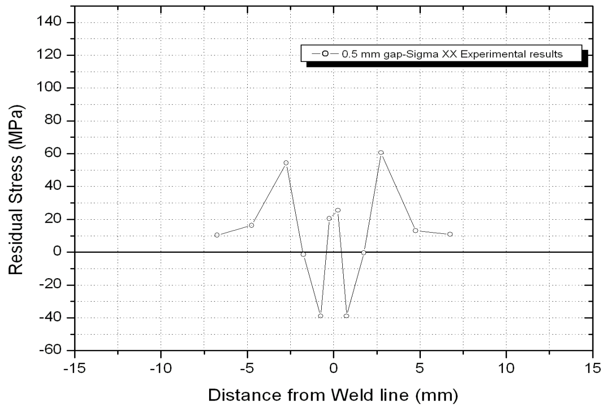

Fig. 2.11 Experimental results of residual stress

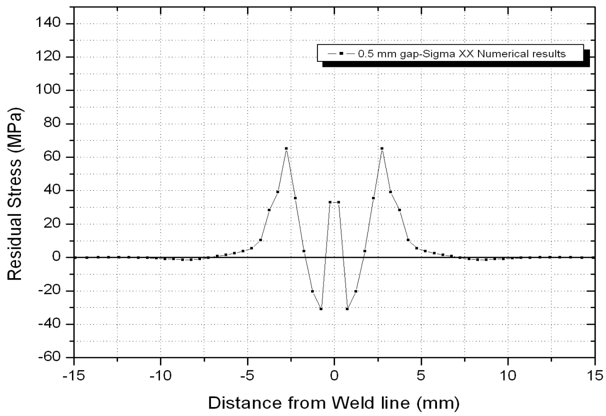

Fig. 2.12 Numerical results of residual stress

CHAPTER 3. Experiments of Nd:YAG laser+MIG Hybrid welding

3.1 Various Parameters of Hybrid welding Process

Welding parameters of hybrid welding are most complicated than any other welding methods because two welding methods were combined. Interactional parameters in two welding should be considered, not to be included of each parameter.

3.1.1 MIG welding

- Welding current
- Welding arc voltage
- Polarity
- Welding speed
- Electrode extension
- Electrode diameter
- Angle of torch
- Shielding gas

Welding current is related to metal transfer mode which is divided into three, short-circuiting, globular, spray transfer mode. In aluminum case, spray mode is suitable. Arc voltage is continuous with current directly and it is increased with arc length. Also it is under the control the shielding gas and electrode extension. The wide and flat bead is formed when voltage is increasing. Low voltage increases weld reinforcement, excess voltage causes unstable arc, spatter, porosity and undercut.

Generally MIG welding of aluminum uses direct current electrode positive (DCEP) for stable arc, less spatter, sound welding bead shape and deep penetration.
The more welding speed increases, the more decreased heat input and deposition rate became. When welding speed increases at starting point, welding penetration can increase because arc affects base metal directly. But if welding speed increases more and more, welding penetration will decrease and undercut can occur.

Electrode extension is a distance from the tip of contact tube to the tip of an electrode wire. If electrode extension becomes long, melting rate is increased by Joule effect. Usually electrode extension ranges from 13 to 25mm for spray and globular transfer mode. When MIG welding the angle of arc torch should be within 15°. Optimum angle, from 10° to 15°, has been used.

The chemical composition of electrode should be almost same as base metal. Usual electrode diameter in MIG welding are 0.8mm, 1.2mm and 1.6mm. 1.2mm and 1.6mm are used in thick plates to make wide weld pool, but high current is needed. In this present experiment, 1.6mm diameter electrode wire has been selected.

Shielding gas is effective for arc stability, metal transfer mode, bead shape and melting rate. Pure Ar, He and CO_2 are used commonly. Ar and He, which are inert gases, are used for light in weight metal alloys, for example nickel and copper alloys. He gas has higher ionization tendency than Ar, wide weld pool can be formed but it costs very high. In case of aluminum welding, pure Ar or Ar and He mixture are used.

3.1.2 Nd:YAG Laser welding

- Incident laser beam power
- Incident laser beam diameter
- Focal length
- Absorptivity
- Welding speed

The depth of penetration with laser welding is directly related to the power density of the laser beam and is a function of incident beam power and beam diameter.
Laser beam diameter is the important factor which determines the power density. For example, beam diameter is related to the focal length, power density of beam diameter is changed when varying the focal length. Also if focal point is above(+) or under(-) the surface, the position of incident beam focal point will be different and the power density will be low.

Absorptivity is one of standards which measure the efficiency of laser welding. The infrared absorption of metals largely depends on the conductivity absorption by free electrons. Therefore, absorptivity is a function of the electrical resistivity of the substrate material. Also absorptivity is depend upon surface condition, temperature-dependent of material and wavelength of laser beam. In such an aluminum case, according to increment of alloyed elements in pure aluminum, electrical resistivity increases.[9]

The penetration in the laser weld is consistently less than that obtained with an electron beam, but the relative difference between the two penetration depths diminishes as the welding speed is increased. Because the time to form a void or keyhole depends on the illumination time for a particular area on the surface of the workpiece as the welding speed is increased. When this occurs, the average power dissipated in the sheet is expected to drop because the keyhole is no longer a completely effective trap for the incident laser radiation.[10]

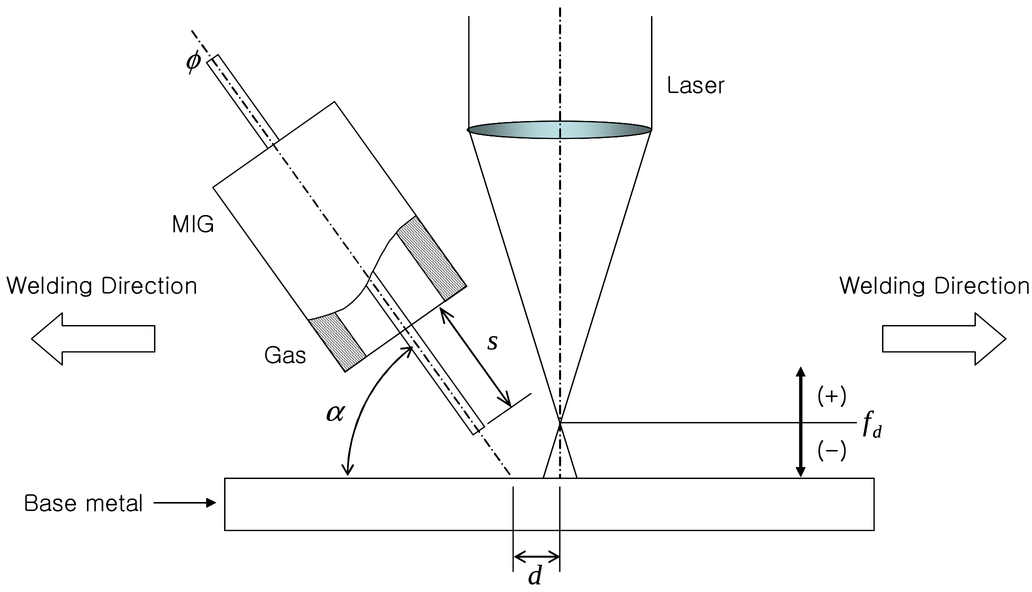

Fig. 3.1 Considered parameters of Nd:YAG laser+MIG hybrid welding

3.2 Hybrid welding Experiments

As previously stated, considering various parameters, butt joint of A6061 by laser+MIG hybrid welding were carried out.

ABB 6-axis robot used in these experiments was with a Trumpf CW 3kW Nd:YAG laser and MIG torch on the robot head for making hybrid welding process. Fig. 3.2 shows the robot of laser+MIG hybrid welding, Fig. 3.3 is the head of laser+MIG hybrid welding.

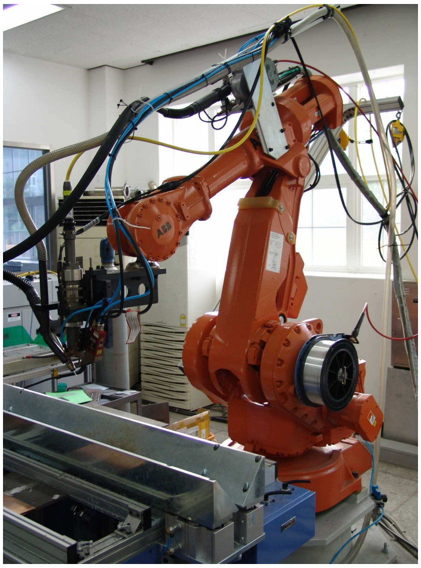

Fig. 3.2 Hybrid welding Robot

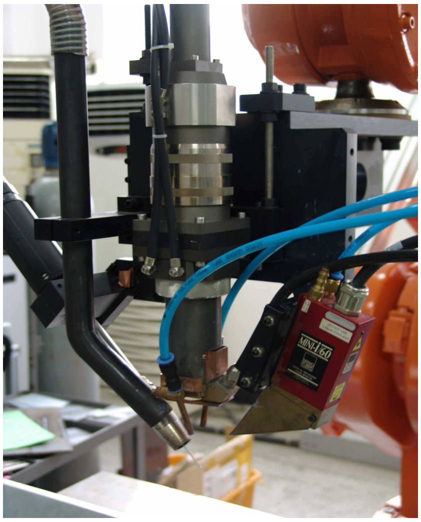

Fig. 3.3 Laser-arc Hybrid welding Head

Only Ar was used for shielding gas which was supplied through a MIG torch located at the side of laser head and nozzles located at the side of laser head.

A Specimen size was 100mm wide, 250mm long and 5mm thickness. Before welding the surface of specimen was cleaned using a stainless steel wire brush for aluminum and degreased by wiping with methyl alcohol.

Determined optimum welding conditions of laser+MIG hybrid welding are shown by Table 3.1. The maximum laser power was used and laser leading process was selected. Because The bead shape formed by laser leading was much cleaner and more sound than MIG leading in hybrid welding. When defocused depth was -2mm, full penetration was obtained.

Table 3.1 Laser-arc hybrid welding Conditions

Welding condition		Values
MIG	Current	195A
	Voltage	26V
	Shielding gas	Ar 13ℓ/min
	CTWD	15mm
	Dia. of electrode	1.6mm, A4043
	Angle of torch(α)	45°
Nd:YAG Laser	Power	3kW
	Focal length(f_d)	221mm
	Shielding gas	Ar 5ℓ/min

· Laser-arc Distance(d) : 3mm

· Leading process : Laser welding

· Defocused depth : -2mm

The top and bottom bead shapes according to joint gap and welding speed were investigated. As shown in Table 3.2, the width of bead became wide by increasing the joint gap. When welding speed is 0.85m/min and gap is 0.5mm, the most sound bead shape and full penetration were formed. But full penetration could not be obtained in 0.9m/min speed, only full penetration could be partially acquired in 0.5mm gap.

Table 3.2 Bead surface condition of hybrid welds

Welding Speed (m/min)	Gap(mm)	Top Bead	Bottom Bead
0.8m/min	0.5mm	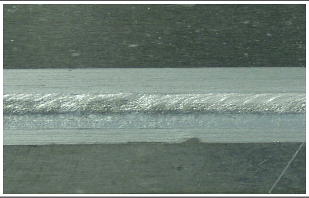	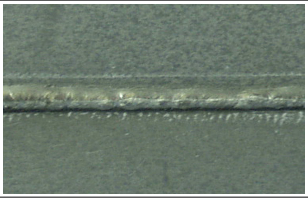
	1mm		
0.85m/min	0mm	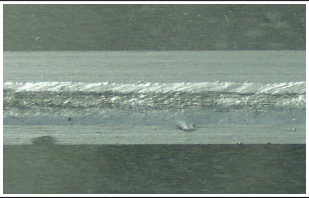	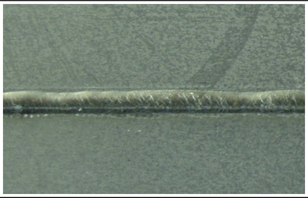
	0.5mm	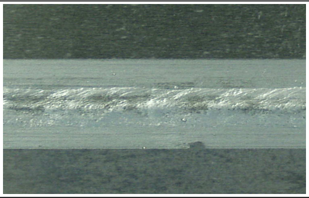	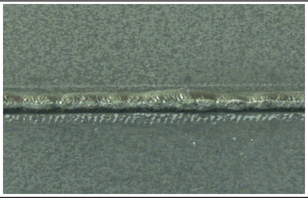
0.9m/min	0mm	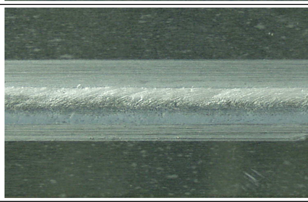	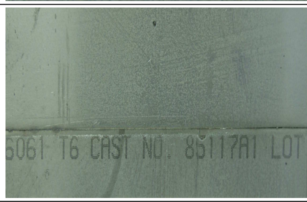
	0.5mm		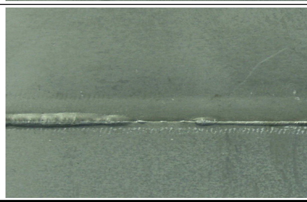

Table 3.3 Cross Section of hybrid welds

Welding Speed (m/min)	Gap(mm)	Cross Section
0.8m/min	0.5mm	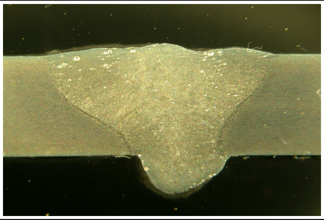
	1mm	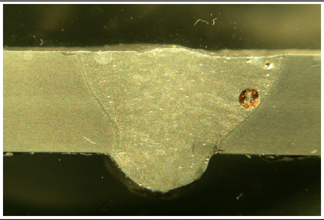
0.85m/min	0mm	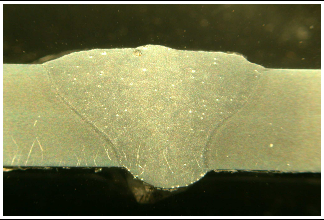
	0.5mm	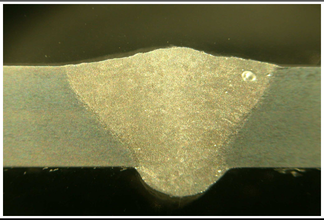

Cross sections of laser+MIG hybrid welds are shown in Table 3.3. Porosity was found out in all sections but the number of porosity was less than conventional aluminum welding, MIG. Because while hybrid welding, hydrogen gas which remains on the aluminum surface couldn't escape from the weld pool due to fast cooling of laser welding in hybrid welding. Fig. 3.4 and Fig. 3.5 show the porosity of cross section in conventional welding and laser+MIG hybrid welding.

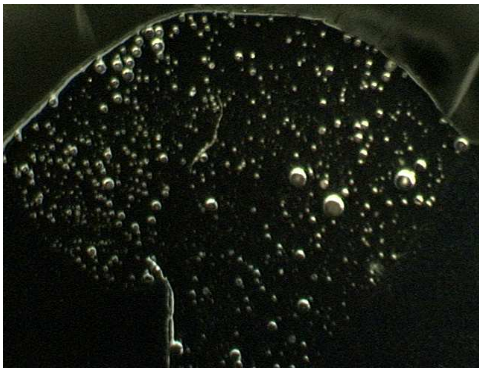

Fig. 3.4 Cross section of MIG welds

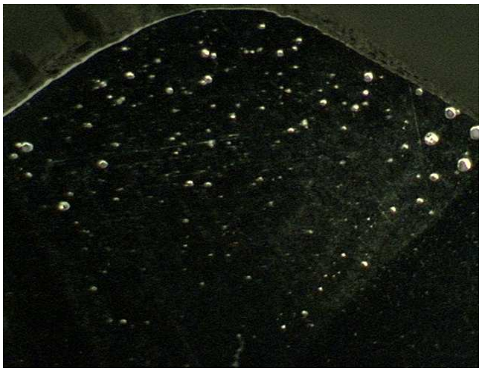

Fig. 3.5 Cross section of hybrid welds

CHAPTER 4. Mechanical Characteristics of Hybrid welds

4.1 Hardness Test in Hybrid welds

The hardness of transverse section which was welded by optimum parameters was measured by vickers hardness tester. A load of 0.5kgf and a spacing of 0.1mm and 0.5mm between the indentations were used. The measured hardness values are shown in Fig. 4.1.

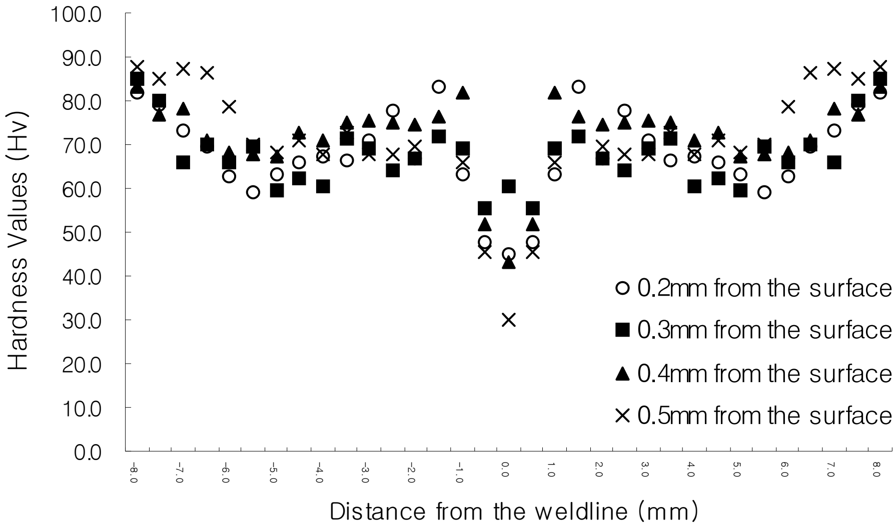

Fig. 4.1 Hardness value in Nd:YAG+MIG hybrid welds

As shown in Fig. 4.1, lowest value of hardness occurred in weld metal. Where as toward the base metal, hardness value increases. This phenomenon can be explained by alloying elements and heat input. In other words, mechanical properties of welded materials has been affected by heat input which vaporizes the alloying elements.[11] In case of Al 6000 series, Mg and

Si are alloyed in pure aluminum, especially Mg is the main element for strengthening the aluminum. While welding, Mg is vaporized by heat input, thus the strength of weld metal decreases.
Comparing the hardness value of each area, hardness value of HAZ mediates between weld metal and base metal. Hardness of weld metal was between 50~60 Hv, HAZ was 60~80 Hv and base metal was 80~90 Hv.

4.2 Comparison of Bead Geometry in Hybrid Welds

Bead geometry of Nd:YAG laser+MIG hybrid welds was compared between numerical simulation and experimental results. Fig. 4.2 shows the numerically simulated geometry in hybrid welds when temperature was maximum. (t=1.8sec) Fig. 4.3 shows the microscopic view of the hybrid weldment.

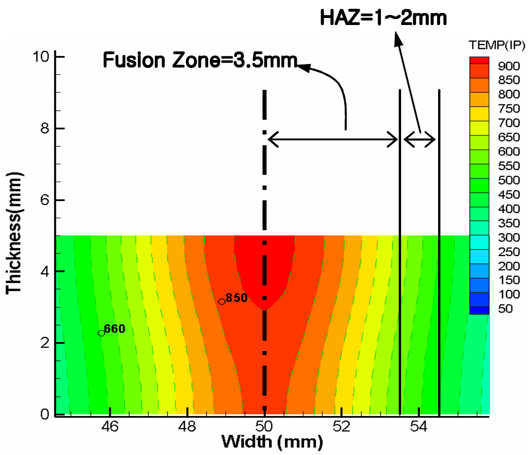

Fig. 4.2 Geometry of numerical welds

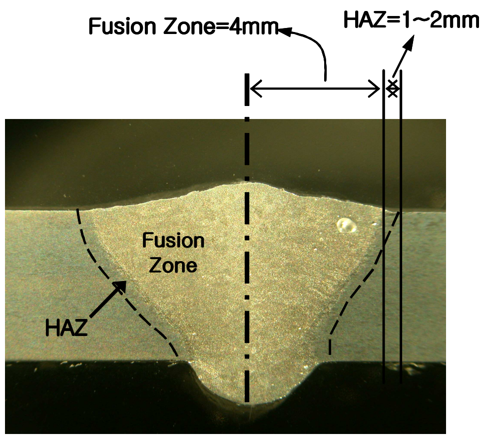

Fig. 4.3 Geometry of experimental welds

From the temperature contour, fusion zone boundary is represented by contour with melting point temperature. HAZ zone is with in range of melting point temperature contour and HAZ temperature limit. Thus width of the top bead was 3.5mm and HAZ of 2mm which where comparable with actual bead and HAZ geometry.

CHAPTER 5. Conclusion

In this study, thermal behavior and mechanical characteristics of Nd:YAG laser+MIG hybrid welding in A6061 was investigated for improving weldability of aluminum alloys. And the application in industrial fields has been justified.

1) As a result of this study, optimum condition was determined by experiments. The optimum welding conditions were as follows: laser power 3kW, arc current 195A, arc voltage 26V, welding speed 0.85m/min and 0.5mm gap tolerance. Also these conditions were obtained in laser leading case, weld beads in laser leading case were found much better than arc leading case. And if the laser power is higher than 3kW, the speed could be further increased. But porosity was generated in all conditions.

2) Heat transfer and temperature history could be predicted by numerical simulation using FEM. Combination heat source model of split type (volume by GMAW and volume by CW Nd:YAG laser) has been considered to analyze the heat source of hybrid welding.

3) Thermal history that with high temperature gradient has been obtained from the numerical simulation results. This phenomena can be explained by laser welding which has a higher cooling time compared to arc welding.

4) Numerically determined longitudinal residual stress has been compared to experimentally determined residual stress of hybrid welds. It was confirmed that numerical value matched the experimental value. Maximum residual stress was about 70Mpa, almost 25% of yield strength in aluminum alloys

5) Thus a preliminary study on the hybrid welding application in A6061-T6

alloys, has been successfully carried out.

Reference

1. AWS Welding Handbook Vol 3, Materials and Applications - Part 1, p.10
2. AWS Welding Handbook Vol 3, Materials and Applications - Part 1, p.2
3. ASM Handbook Vol 2, "Properties and Selection; Nonferrous Alloys and Special-Purpose Materials", p.32
4. ASM Specialty Handbook "Aluminum and Aluminum Alloys", p.10
5. ASM Han dbook Vol 2, "Properties and Selection; Nonferrous Alloys and Special-Purpose Materials", p.20
6. 대한용접학회, 용접 · 접합 편람, pp.249
7. Young-Pyo Kim, "The Study on Mechanical Behavior of Butt Joints in Al-Mg Alloys by Hybrid(CW Nd:YAG Laser+MIG) Welding", Ph.D. Thesis, Chosun University, Korea, February. 2005
8. H.S. Bang and Y.P. Kim. "Fundamental Study on The Heat Input Model of Hybrid Welding for The Finite Element Analysis". Proceeding of the 2003 Autumn Annual Meeting of Korean Welding Society, pp.36~38, 2003.(In Korea)
9. ASM International handbook Vol. 6 Welding, Brazing, and Soldering, pp. 265
10. ASM International handbook Vol. 6 Welding, Brazing, and Soldering, pp. 266
11. 대한용접학회, 용접 · 접합 편람, pp.253

Acknowledgments

어느 덧, 석사 과정이라는 관문을 마무리 지어야 할 이 시점에서 제가 얼마나 열심히 생활했고 무엇을 얻었는지 생각하게 되었습니다. 후회되는 시간들도 많고 아쉬운 점들도 많지만 그래도 저를 믿고 지켜봐 주신 분들이 계셨기에 오늘의 값진 결실을 맺을 수 있었다고 생각합니다.

학부시절, 천방지축이었던 저를 끊임없이 질책하면서도 자신감을 가질 수 있는 기회를 주신 방한서 교수님께 먼저 깊은 감사의 말씀을 올립니다. 또한 저에게 지도와 관심을 베풀어 주신 윤덕영 교수님, 박제웅 교수님, 이귀주 교수님, 권영섭 교수님, 좌순원 교수님, 방희선 교수님께도 감사드리며, 무엇보다도 베푸는 삶을 강조하시며 저를 이끌어 주신 김도정 교수님께 감사의 마음을 전하고 싶습니다.

그리고 석사과정을 함께 밟으면서 철없는 저를 챙겨주며 고생한 나의 동기들(^^), 호경오빠, 준기오빠, 재선오빠와 항상 우리들을 감싸준 종인오빠, 술과 함께 많은 이야기를 나눴던 Rajesh 오빠, 그리고 그 외 용접 · 구조 연구실 선배님들께 감사드리며, 공부 열심히 하라고 저를 격려해 주신 주위 선 · 후배, 친구들에게 고개 숙여 감사드립니다.

마지막으로, 아무 말 없이 항상 묵묵하게 저를 지켜봐 주신 부모님과 언니이자 누나로서 이제까지 해준 건 없지만 잘 따라줬던 선영이와 보영이에게 사랑한다는 말과 함께 앞으로 부모님께 효도하면서 언제나 함께 할 거라 약속드리며 이 논문을 받칩니다.

2006년 12월

정 은 영 올림

저작물 이용 허락서

학 과	선박해양공학	학 번	20057145	과 정	석사
성 명	한글: 정 은 영 한문 : 鄭 垠 永 영문 : Jeong Eun-Young				
주 소	광주광역시 남구 봉선2동 삼익아파트 2차 203동 1003호				
연락처	E-MAIL : icerock@naver.com				
논문제목	한글 : 하이브리드(Nd:YAG+MIG) 용접을 이용한 알루미늄(Al-Mg-Si)합금의 열적 거동 및 역학적 특성에 관한 연구				
	영문 : A Study on Thermal Behavior and Mechanical characteristics in Hybrid welding (Nd:YAG Laser+MIG) of Al-Mg-Si alloys				

본인이 저작한 위의 저작물에 대하여 다음과 같은 조건아래 조선대학교가 저작물을 이용할 수 있도록 허락하고 동의합니다.

- 다 음 -

1. 저작물의 DB구축 및 인터넷을 포함한 정보통신망에의 공개를 위한 저작물의 복제, 기억장치에의 저장, 전송 등을 허락함
2. 위의 목적을 위하여 필요한 범위 내에서의 편집・형식상의 변경을 허락함. 다만, 저작물의 내용변경은 금지함.
3. 배포・전송된 저작물의 영리적 목적을 위한 복제, 저장, 전송 등은 금지함.
4. 저작물에 대한 이용기간은 5년으로 하고, 기간종료 3개월 이내에 별도의 의사 표시가 없을 경우에는 저작물의 이용기간을 계속 연장함.
5. 해당 저작물의 저작권을 타인에게 양도하거나 또는 출판을 허락을 하였을 경우에는 1개월 이내에 대학에 이를 통보함.
6. 조선대학교는 저작물의 이용허락 이후 해당 저작물로 인하여 발생하는 타인에 의한 권리 침해에 대하여 일체의 법적 책임을 지지 않음
7. 소속대학의 협정기관에 저작물의 제공 및 인터넷 등 정보통신망을 이용한 저작물의 전송・출력을 허락함.

2006년 12 월 12 일

저작자: 정 은 영 (서명 또는 인)

조선대학교 총장 귀하